JOURNAL OF SPACECRAFT AND ROCKETS
Vol. 37, No. 5, September–October 2000

Development of Mechanical Models for Propellant Sloshing in Teardrop Tanks

M. Utsumi*
Ishikawajima–Harima Heavy Industries Company, Ltd., Tokyo 135-0061, Japan

An analytical method is extended to the sloshing problem in which the static liquid domain is nonaxisymmetrical. A feature of this method is that the characteristic function can be analytically determined by using spherical coordinates according to the position of the contact line of the static liquid surface with the tank wall. As an example, sloshing in a teardrop tank is considered. The case in which the gravity force caused by the propulsive acceleration of the vehicle prevails over the centrifugal and Coriolis forces due to spinning is studied. Mechanical models are developed in two orthogonal directions normal to the tank axis.

Nomenclature

a	=	radius of spherical part of tanks (Fig. 1), m
b	=	$a/\sin\theta_C$ (Fig. 1), m
$\ddot{f}_{\tilde{x}}(t)$, $\ddot{f}_{\tilde{y}}(t)$	=	accelerations of tank in $\tilde{x}$ and $\tilde{y}$ directions, m/s^2
g	=	gravity acceleration due to vehicle propulsion, m/s^2
H	=	distance between x' axis and apex of conical part of tank (Fig. 1), m
$k_{\tilde{x}}$, $k_{\tilde{y}}$	=	spring constants of mechanical models (Fig. 2), N/m
L	=	distance between z axis and apex of conical part of tank (Fig. 1), m
$l_{0\tilde{x}}$, $l_{0\tilde{y}}$	=	$\tilde{z}$ coordinates of attachment points of fixed masses of mechanical models (Fig. 2), m
$l_{1\tilde{x}}$, $l_{1\tilde{y}}$	=	$\tilde{z}$ coordinates of attachment points of slosh masses of mechanical models (Fig. 2), m
M	=	undisturbed liquid surface
$m_{0\tilde{x}}$, $m_{0\tilde{y}}$	=	fixed masses of mechanical models (Fig. 2), kg
$m_{1\tilde{x}}$, $m_{1\tilde{y}}$	=	slosh masses of mechanical models (Fig. 2), kg
$\boldsymbol{N}_F$	=	unit normal vector of F pointing into liquid domain
$\boldsymbol{N}_M$	=	unit normal vector of M pointing into liquid domain
$\boldsymbol{N}_W$	=	unit normal vector of W pointing outward from liquid domain
p	=	pressure, N/m^2
p_{imp}	=	impulsive pressure due to excitation of the tank, N/m^2
p_{slo}	=	slosh pressure due to liquid motion relative to the tank, N/m^2
p_{st}	=	static pressure, N/m^2
$q(t)$	=	modal coordinate
(R, θ, φ)	=	spherical coordinates (Fig. 4)
$R_F(\theta, \varphi, t)$	=	R coordinate of disturbed liquid surface, m
$R_M(\theta)$	=	R coordinate of undisturbed liquid surface, m
$R_W(\theta)$	=	R coordinate of tank wall, m
u_R, u_θ, u_φ	=	displacement components of liquid relative to tank, m
v_R, v_θ, v_φ	=	velocity components of liquid relative to tank, m/s
W	=	tank wall
(x, y, z)	=	coordinates fixed to spinning tank system (Fig.1), m
α	=	circumferential coordinate of specified tank (Fig. 1)
γ	=	tilt of tank axis $\tilde{z}$ from $-z$ direction (Fig. 1)
ε	=	1 or -1 when $\tilde{z}'$ coordinate of the origin O is positive or negative, respectively (Fig. 4)
ζ	=	liquid surface displacement, m
Θ_{mk}	=	characteristic function determined by Eqs. (A4) and (A6)
$\bar{\theta}$	=	maximum value of θ
θ_C	=	half the apex angle of conical part of tank (Fig. 1)
λ_{mk}	=	characteristic value, 1/m
ρ	=	density of liquid, kg/m^3
ϕ	=	velocity potential (relative motion to tank), m^2/s
φ_E, θ_E, ψ_E	=	Euler's angles for determining spherical coordinates (Figs. 3 and 4)
ω	=	angular frequency of excitation, rad/s

Introduction

THE study of sloshing has stimulated the interest of researchers for a long time because sloshing significantly affects the dynamics and control analysis of the satellite.[1] In a previous paper,[2] the author reported a new semianalytical method for the sloshing problem for an arbitrary axisymmetrical static liquid domain. The advantage of this method over conventional numerical approaches is that little computation time and cost are required because the characteristic functions can be analytically determined by using spherical coordinates according to the position of the contact line of the static liquid surface with the tank wall. However, the static liquid domain is not necessarily axisymmetrical in engineering applications. The purpose of this study is to extend the previously reported method to a case in which the static liquid domain exhibits a marked nonaxisymmetrical shape. As an example, sloshing in a teardrop tank (Fig. 1) is considered.

This paper addresses a fundamental case in which the spin rate of the tank around the z axis is very low and hence the centrifugal and Coriolis accelerations can be neglected, for the following two reasons. First, the possibility of the extension of the previously reported method can be examined readily using the irrotational flow theory. Second, such a case may be realized frequently for satellites requiring the use of teardrop tanks, whose purpose is to hold the propellant at the outlet of the tank (the apex of the conical surface) for various combinations of the propulsive acceleration and the spin rate. For example, the lunar exploration satellite LUNAR-A, which is a main motivation of this work, has a mission to detach some objects every few weeks and send them to the moon for examination of physical conditions at various places on the lunar surface.[3] Except when it detaches the objects, the spin rate is very low and hence the sloshing is dominated by the propulsive acceleration.

Solution Method

Cartesian Coordinate Systems and Problem Statement

The computational model is shown in Fig. 1, where $Cxyz$ is a coordinate system fixed to the tank system. The liquid surface is perpendicular to the z axis. Two Cartesian coordinate systems

Received 20 April 1999; revision received 22 March 2000; accepted for publication 1 April 2000.

*Section Manager, Machine Element Department, Research Institute, 3-1-15 Toyosu, Koto-ku.

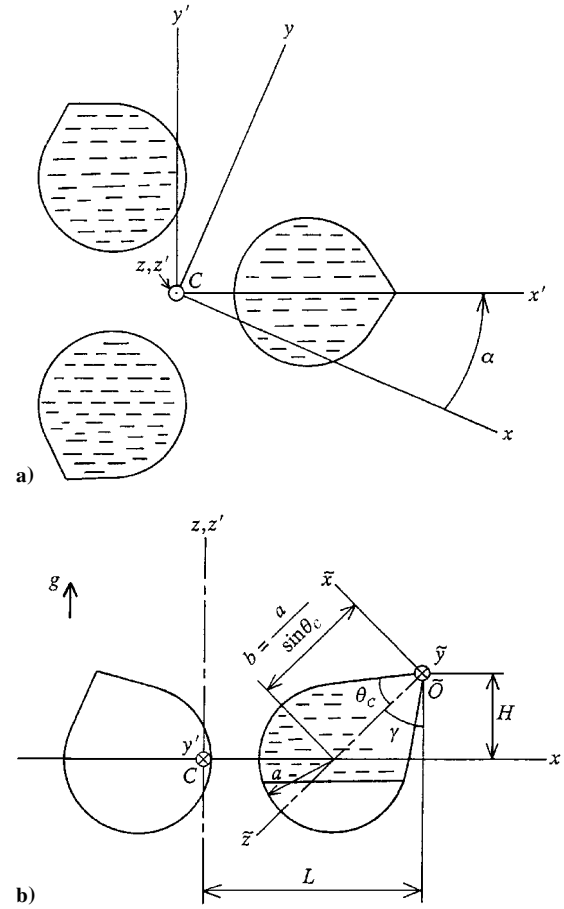

Fig. 1 Teardrop tank system. (Teardrop-shaped tanks are formed by spherical and conical surfaces and arranged in circumferential 120-deg pitch with one generatrix of the conical surfaces nearly parallel to the z axis.)

are defined successively, according to the position and the attitude of a specified tank. First, define the coordinate system $Cx'y'z'$ by rotating $Cxyz$ by the angle α around the z axis (Fig. 1a):

$$\begin{Bmatrix} x \\ y \\ z \end{Bmatrix} = \begin{bmatrix} \cos\alpha & -\sin\alpha & 0 \\ \sin\alpha & \cos\alpha & 0 \\ 0 & 0 & 1 \end{bmatrix} \begin{Bmatrix} x' \\ y' \\ z' \end{Bmatrix} \tag{1}$$

where α denotes the circumferential coordinate of the specified tank measured from the x axis. Second, as shown in Fig. 1b, set the coordinate system $\tilde{O}\tilde{x}\tilde{y}\tilde{z}$ for the specified tank by rotating $Cx'y'z'$ by the angle $\pi - \gamma$ around the y' axis and shifting the origin C by length L in the x' direction and height H in the z' direction:

$$\begin{Bmatrix} x' \\ y' \\ z' \end{Bmatrix} = \begin{bmatrix} -\cos\gamma & 0 & -\sin\gamma \\ 0 & 1 & 0 \\ \sin\gamma & 0 & -\cos\gamma \end{bmatrix} \begin{Bmatrix} \tilde{x} \\ \tilde{y} \\ \tilde{z} \end{Bmatrix} + \begin{Bmatrix} L \\ 0 \\ H \end{Bmatrix} \tag{2}$$

The purpose here is to develop mechanical models as shown in Fig. 2 for the specified tank. The mechanical model shown in Fig. 2a is designed such that the frequency responses of the resultant force in the $\tilde{x}$ direction and the resultant moment about the $\tilde{y}$ axis to the excitation in the $\tilde{x}$ direction coincide with those of the actual sloshing system. On the other hand, the parameters of the mechanical model shown in Fig. 2b are determined from the condition that the frequency responses of the resultant force in the $\tilde{y}$ direction and the resultant moment about the $\tilde{x}$ axis to the excitation in the $\tilde{y}$ direction are the same as those of the actual sloshing system.

The following assumptions are used in the analysis: 1) The liquid motion is inviscid and incompressible. 2) The tank is rigid. 3) The oscillatory motion of the liquid relative to the tank is small enough to be represented within the framework of the linear theory.

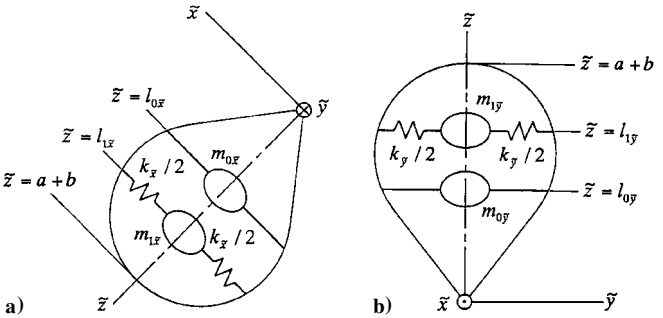

Fig. 2 Mechanical models for excitation in the a) $\tilde{x}$ direction ($m_{1\tilde{x}}$, slosh mass; $m_{0\tilde{x}}$, fixed mass) and b) $\tilde{y}$ direction ($m_{1\tilde{y}}$, slosh mass; $m_{0\tilde{y}}$, fixed mass).

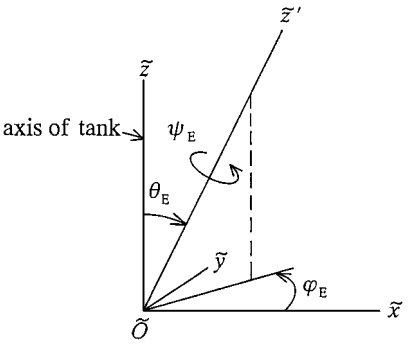

Fig. 3 Euler angles determining the relation between the coordinates $(\tilde{x}, \tilde{y}, \tilde{z})$ and $(\tilde{x}', \tilde{y}', \tilde{z}')$ with respect to which spherical coordinates are defined by Eq. (4).

Spherical Coordinates

We define the coordinate system $\tilde{O}\tilde{x}'\tilde{y}'\tilde{z}'$ by rotating $\tilde{O}\tilde{x}\tilde{y}\tilde{z}$ by the Euler angles (Fig. 3)

$$\begin{Bmatrix} \tilde{x} \\ \tilde{y} \\ \tilde{z} \end{Bmatrix} = \begin{bmatrix} c_{E11} & c_{E12} & c_{E13} \\ c_{E21} & c_{E22} & c_{E23} \\ c_{E31} & c_{E32} & c_{E33} \end{bmatrix} \begin{Bmatrix} \tilde{x}' \\ \tilde{y}' \\ \tilde{z}' \end{Bmatrix} \tag{3a}$$

where

$$\begin{aligned} c_{E11} &= \cos\varphi_E \cos\theta_E \cos\psi_E - \sin\varphi_E \sin\psi_E \\ c_{E12} &= -\cos\varphi_E \cos\theta_E \sin\psi_E - \sin\varphi_E \cos\psi_E \\ c_{E13} &= \cos\varphi_E \sin\theta_E \\ c_{E21} &= \sin\varphi_E \cos\theta_E \cos\psi_E + \cos\varphi_E \sin\psi_E \\ c_{E22} &= -\sin\varphi_E \cos\theta_E \sin\psi_E + \cos\varphi_E \cos\psi_E \\ c_{E23} &= \sin\varphi_E \sin\theta_E, \qquad c_{E31} = -\sin\theta_E \cos\psi_E \\ c_{E32} &= \sin\theta_E \sin\psi_E, \qquad c_{E33} = \cos\theta_E \end{aligned} \tag{3b}$$

We then set the circumferential coordinate φ around the $\tilde{z}'$ axis, as shown in Fig. 4, and introduce spherical coordinates $ORθφ$ for each subdivided section $\varphi_j \le \varphi \le \varphi_j + \Delta\varphi (\Delta\varphi = 2\pi/\mathrm{N}, \varphi_j = (j-1)\Delta\varphi, j = 1, 2, \ldots, \mathrm{N})$ such that

$$\begin{aligned} \tilde{x}' &= R\sin\theta\cos\varphi, \qquad \tilde{y}' = R\sin\theta\sin\varphi \\ \tilde{z}' &= h - \varepsilon R\cos\theta, \qquad (0 \le \theta \le \bar{\theta}) \end{aligned} \tag{4}$$

The origin $O(\tilde{z}' = h)$ is chosen as the intersection of the $\tilde{z}'$ axis and the line that is included in the plane $\varphi = \varphi_j$, and is tangent to the tank wall at the contact line of the undisturbed liquid surface with the tank wall. Examples of such spherical coordinates are shown in Fig. 4 for some subdivided section numbers $j = j_1$, j_2, and j_3. In terms of the spherical coordinates, we can express the undisturbed

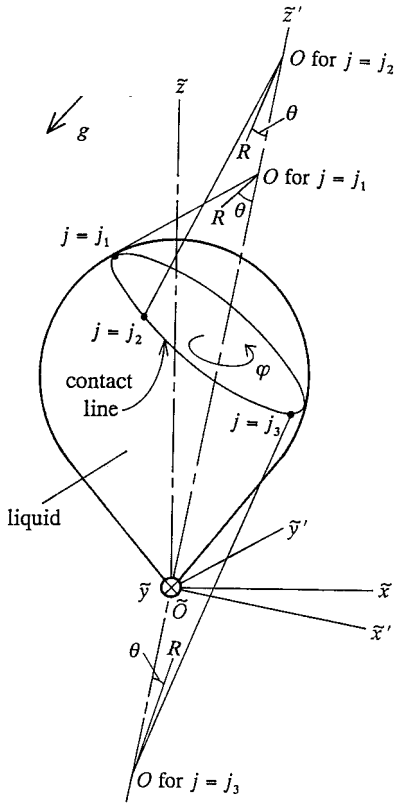

Fig. 4 Spherical coordinate systems $OR\theta\varphi$ applied according to the position of the contact line of the liquid surface with the tank wall.

liquid surface M, the disturbed liquid surface F, and the container wall W as

$$M\text{: } R = R_M(\theta) \tag{5}$$

$$F\text{: } R = R_F(\theta, \varphi, t) = R_M(\theta) + \zeta(\theta, \varphi, t) \tag{6}$$

$$W\text{: } R = R_W(\theta) \tag{7}$$

The symbol j representing the subsection number is omitted to keep the notations uncomplicated. Evaluation of the actual form of the functions $R_M(\theta)$ and $R_W(\theta)$ is straightforward.[3]

Note that the axis of the spherical coordinates is chosen to be the $\tilde{z}'$ axis instead of the $\tilde{z}$ axis, the center line of the tank. If we choose the $\tilde{z}$ axis as an axis of the spherical coordinates, the intersection of the tank wall and the $\tilde{z}$ axis is inside the liquid domain for high liquid-filling levels, and therefore we cannot use Eqs. (5) and (6). Thus, the relation between the $\tilde{z}'$ and $\tilde{z}$ axes must be flexibly adjusted by using the Euler angles (Fig. 3).

The system of characteristic functions can be determined analytically by using the spherical coordinates, as explained in detail later. Furthermore, the liquid surface displacement ζ at the tank wall can be made tangential to the tank wall. Namely, the compatibility condition required for the surface displacement at the tank wall can be satisfied. Note that only one component of the surface displacement vector needs to be considered to satisfy the compatibility condition.

In terms of the spherical coordinates, the unit normal vectors and the surface elements, which are used later, are expressed as

$$\boldsymbol{N}_F = \varepsilon\left[R_F\boldsymbol{e}_R - \left(\frac{\partial R_F}{\partial\theta}\right)\boldsymbol{e}_\theta - \left(\frac{1}{\sin\theta}\frac{\partial R_F}{\partial\varphi}\right)\boldsymbol{e}_\varphi\right]\Bigg/ \left[R_F^2 + \left(\frac{\partial R_F}{\partial\theta}\right)^2 + \left(\frac{1}{\sin\theta}\frac{\partial R_F}{\partial\varphi}\right)^2\right]^{\frac{1}{2}} \tag{8}$$

$$\boldsymbol{N}_W = \varepsilon\left[R_W\boldsymbol{e}_R - \frac{\mathrm{d}R_W}{\mathrm{d}\theta}\boldsymbol{e}_\theta\right]\Bigg/\left[R_W^2 + \left(\frac{\mathrm{d}R_W}{\mathrm{d}\theta}\right)^2\right]^{\frac{1}{2}} \tag{9}$$

$$\mathrm{d}F = R_F\left\{\left[R_F^2 + \left(\frac{\partial R_F}{\partial\theta}\right)^2\right]\sin^2\theta + \left(\frac{\partial R_F}{\partial\varphi}\right)^2\right\}^{\frac{1}{2}}\mathrm{d}\theta\,\mathrm{d}\varphi \tag{10}$$

$$\mathrm{d}W = R_W\left\{R_W^2 + \left(\frac{\mathrm{d}R_W}{\mathrm{d}\theta}\right)^2\right\}^{\frac{1}{2}}\sin\theta\,\mathrm{d}\theta\,\mathrm{d}\varphi \tag{11}$$

Equations (8) and (9) can be derived from Eqs. (6) and (7) by using the theorem that the normal vector of a surface expressed in the form $f(R, \theta, \varphi, t) = 0$ is given by grad f. Equation (10) can be obtained by determining the position vector of the surface F:

$$\boldsymbol{X} = \{R_F\sin\theta\cos\varphi,\ R_F\sin\theta\sin\varphi,\ h - \varepsilon R_F\cos\theta\}^T \tag{12}$$

and estimating the area of the parallelogram formed by the infinitesimal tangential vectors along the θ and φ directions by

$$\mathrm{d}F = \left|\frac{\partial\boldsymbol{X}}{\partial\theta}\times\frac{\partial\boldsymbol{X}}{\partial\varphi}\right|\mathrm{d}\theta\,\mathrm{d}\varphi \tag{13}$$

Variational Principle

The slosh analysis is performed based on a variational principle for the irrotational sloshing problem presented in a previous paper.[2] This variational principle can be expressed as

$$\int_{t_1}^{t_2}\Bigg\{\rho\iiint_V\nabla^2\phi\,\delta\phi\,\mathrm{d}V - \rho\iint_W\nabla\phi\cdot\boldsymbol{N}_W\delta\phi\,\mathrm{d}W - \rho\iint_F\left[\frac{\partial\zeta}{\partial t}\cos(\boldsymbol{N}_F, R) - \nabla\phi\cdot\boldsymbol{N}_F\right]\delta\phi\,\mathrm{d}F - \iint_F\left[-\rho\frac{\partial\phi}{\partial t} + \rho g(z - z_M) + p_{\mathrm{imp}}\right]\delta\zeta\cos(\boldsymbol{N}_F, R)\,\mathrm{d}F - \rho\delta G\iint_F\frac{\partial\zeta}{\partial t}\cos(\boldsymbol{N}_F, R)\,\mathrm{d}F\Bigg\}\mathrm{d}t = 0 \tag{14}$$

where ϕ is the velocity potential describing the liquid motion relative to the tank, z_M is the z coordinate of the static liquid surface, G is an arbitrary time-dependent function appearing in the pressure equation, and p_{imp} is the impulsive pressure resulting from the inertial force of the liquid created by the excitation of the tank. The impulsive pressure is given by

$$p_{\mathrm{imp}} = -\rho[\ddot{f}_{\tilde{x}}(t)(\tilde{x} - \tilde{x}_0) + \ddot{f}_{\tilde{y}}(t)(\tilde{y} - \tilde{y}_0)] \tag{15}$$

where $\tilde{x}_0$ and $\tilde{y}_0$ are determined by

$$\tilde{x}_0 = \iint\tilde{x}\,\mathrm{d}M\Big/\iint\mathrm{d}M, \qquad \tilde{y}_0 = \iint\tilde{y}\,\mathrm{d}M\Big/\iint\mathrm{d}M \tag{16}$$

such that the mean value of p_{imp} over the liquid surface M is equal to zero. Since the variations $\delta\phi$, $\delta\zeta$, and δG are arbitrary and independent of one another, Eq. (14) yields the following system of fundamental equations:

$$V\text{: } \nabla^2\phi = 0 \tag{17}$$

$$W\text{: } \nabla\phi\cdot\boldsymbol{N}_W = 0 \tag{18}$$

$$F\text{: } \frac{\partial\zeta}{\partial t}\cos(\boldsymbol{N}_F, R) - \nabla\phi\cdot\boldsymbol{N}_F = 0 \tag{19}$$

$$F\text{: } -\rho\frac{\partial\phi}{\partial t} + \rho g(z - z_M) + p_{\mathrm{imp}} = 0 \tag{20}$$

$$\iint_F\frac{\partial\zeta}{\partial t}\cos(\boldsymbol{N}_F, R)\,\mathrm{d}F = 0 \tag{21}$$

The Laplace equation (17) corresponds to the condition of continuity within the liquid domain. Equation (18) means that the liquid velocity in the direction normal to the rigid tank wall vanishes. Equations (19) and (20) represent, respectively, the kinematic and dynamic boundary conditions on the liquid surface. Equation (21) shows that the liquid volume is constant because the liquid is assumed to be incompressible. Because Eq. (21) can be derived from the other kinematic conditions [Eqs. (17–19)] using Green's theorem, the subsequent analysis uses Eqs. (17–20) as basic equations.

By defining the displacement $\boldsymbol{u}$ of liquid and the slosh pressure p_{slo} such that

$$\boldsymbol{u} = \{u_R, u_\theta, u_\varphi\}^T = \int \{v_R, v_\theta, v_\varphi\}^T \, \mathrm{d}t \tag{22}$$

$$p_{\text{slo}} = -\rho \frac{\partial \phi}{\partial t} \tag{23}$$

we have

$$\nabla \phi = \frac{\partial \boldsymbol{u}}{\partial t} \tag{24}$$

$$\delta\phi = -\int \delta p_{\text{slo}} \frac{\mathrm{d}t}{\rho} \tag{25}$$

Substituting Eqs. (24) and (25) into Eq. (14), integrating by parts with respect to t, and substituting Eqs. (8–11) into the resulting equation leads to the following variational principle expressed in the spherical coordinates:

$$\begin{aligned}
&\int_0^{2\pi}\int_0^{\bar\theta}\varepsilon\int_{R_M}^{R_W} \operatorname{div}\boldsymbol{u}\,\delta p_{\text{slo}} R^2 \sin\theta \,\mathrm{d}R\,\mathrm{d}\theta\,\mathrm{d}\varphi \\
&\quad - \int_0^{2\pi}\int_0^{\bar\theta}\varepsilon\left(R_W u_R|_{R=R_W} - \frac{\mathrm{d}R_W}{\mathrm{d}\theta}u_\theta\bigg|_{R=R_W}\right)\delta p_{\text{slo}}\bigg|_{R=R_W} \\
&\quad \times R_W \sin\theta\,\mathrm{d}\theta\,\mathrm{d}\varphi + \int_0^{2\pi}\int_0^{\bar\theta}\varepsilon\left(R_M u_R|_{R=R_M}\right. \\
&\quad \left. - \frac{\mathrm{d}R_M}{\mathrm{d}\theta}u_\theta\bigg|_{R=R_M} - R_M\zeta\right)\delta p_{\text{slo}}\bigg|_{R=R_M} R_M \sin\theta\,\mathrm{d}\theta\,\mathrm{d}\varphi \\
&\quad - \int_0^{2\pi}\int_0^{\theta}\varepsilon\Big[p_{\text{slo}}|_{R=R_M} + \rho\zeta g\cos(z,R) - \rho(\tilde x - \tilde x_0)\ddot f_{\tilde x}(t) \\
&\quad - \rho(\tilde y - \tilde y_0)\ddot f_{\tilde y}(t)\Big]\delta\zeta R_M^2 \sin\theta\,\mathrm{d}\theta\,\mathrm{d}\varphi = 0
\end{aligned} \tag{26}$$

Modal Functions

We transform the variational principle [Eq. (26)] into a standard eigenvalue problem by the Galerkin method, thereby determining the mode shape functions for p_{slo}, u_R, u_θ, u_φ, and ζ. Because p_{slo} satisfies the Laplace equation, as can be seen from Eqs. (17) and (23), we first determine analytically the admissible function for p_{slo} using the spherical coordinates (see Appendix A). We then use Eqs. (23) and (24) to determine the admissible functions for u_R, u_θ, and u_φ. We can thus obtain

$$p_{\text{slo}}(R,\theta,\varphi,t) = \rho a\omega^2 \bar p_{\text{slo}}(R,\theta,\varphi)e^{i\omega t} \tag{27}$$

$$u_R(R,\theta,\varphi,t) = a\bar u_R(R,\theta,\varphi)e^{i\omega t} \tag{28a}$$

$$u_\theta(R,\theta,\varphi,t) = a\bar u_\theta(R,\theta,\varphi)e^{i\omega t} \tag{28b}$$

$$u_\varphi(R,\theta,\varphi,t) = a\bar u_\varphi(R,\theta,\varphi)e^{i\omega t} \tag{28c}$$

$$\zeta(\theta,\varphi,t) = \bar\zeta(\theta,\varphi)e^{i\omega t} \tag{29}$$

where the spatial terms are given by

$$\begin{Bmatrix} \bar p_{\text{slo}}(R,\theta,\varphi) \\ \bar u_R(R,\theta,\varphi) \\ \bar u_\theta(R,\theta,\varphi) \\ \bar u_\varphi(R,\theta,\varphi) \end{Bmatrix} = \sum_{m=0}^{\infty}\sum_{k=1}^{\infty}\sum_{l=1}^{2}\sum_{q=1}^{2} A_{mklq} \times \begin{Bmatrix} X_{mkl}(R)\Theta_{mk}(\theta)\Phi_{mq}(\varphi) \\ X'_{mkl}(R)\Theta_{mk}(\theta)\Phi_{mq}(\varphi) \\ X_{mkl}(R)\Theta'_{mk}(\theta)\Phi_{mq}(\varphi)/R \\ X_{mkl}(R)\Theta_{mk}(\theta)\Phi'_{mq}(\varphi)/R\sin\theta \end{Bmatrix} \tag{30}$$

$$-\varepsilon\bar\zeta(\theta,\varphi) = \sum_{m=0}^{\infty}\sum_{k=1}^{\infty}\sum_{q=1}^{2} C_{mkq}\Theta_{mk}(\theta)\Phi_{mq}(\varphi) \tag{31}$$

with the following characteristic functions:

$$X_{mkl}(R) = \left(\frac{R}{L_l}\right)^{\alpha_{mkl}} \tag{32}$$

$$\begin{aligned}
\Theta_{mk}(\theta) &= \sin^m\theta F_{\text{GAUSS}}\left(m-\alpha, \alpha+m+1, m+1, \frac{1-\cos\theta}{2}\right) \\
&= \sin^m\theta\left[1 + \sum_{i=1}^{\infty}\frac{(m-\alpha)(m-\alpha+1)\cdots(m-\alpha+i-1)}{1\times 2\times\cdots\times i}\right. \\
&\quad \times \frac{(\alpha+m+1)(\alpha+m+2)\cdots(\alpha+m+i)}{(m+1)(m+2)\cdots(m+i)} \\
&\quad \left.\times\left(\frac{1-\cos\theta}{2}\right)^i\right]
\end{aligned} \tag{33}$$

$$\Phi_{m1}(\varphi) = \cos m\varphi, \qquad \Phi_{m2}(\varphi) = \sin m\varphi \tag{34}$$

The derivation of Eqs. (32) and (33) is explained in Appendix A. Note that the characteristic function $\Theta_{mk}(\theta)$ can be obtained as a solution of the standard Sturm–Liouville-type boundary value problem [Eqs. (A4) and (A6)], despite the complicated shape of the liquid domain, to which numerical methods have been customarily applied in the past. The convergence of the solution [Eq. (33)] is rapid for the following reason: It is known that the Gaussian hypergeometric series $F_{\text{GAUSS}}(a,b,c,x)$ converges for arbitrary values of a, b, and c, provided that $|x|<1$. Hence, the solution [Eq. (33)] converges for $0 \le \theta < \pi$. In the present analysis, the maximum value of θ is smaller than $\pi/2$, as can be seen from Fig. 4. This relation $\theta_{\max} < \pi/2$ ensures rapid convergence of the solution [Eq. (33)]. Thus, the analytical determination of the characteristic functions requires only a small amount of computation time and cost.

Substituting Eqs. (27–29) into Eq. (26), neglecting the excitation terms, and considering variations with respect to the constants A_{mklq} and C_{mkq}, we obtain the frequency equation in the form of the standard eigenvalue problem:

$$(-\omega^2\boldsymbol{M} + \boldsymbol{K})\boldsymbol{X} = 0 \tag{35}$$

The column vector $\boldsymbol{X}$ represents the collection of the constants A_{mklq} and C_{mkq}. For the sake of brevity, the components of the matrices $\boldsymbol{M}$ and $\boldsymbol{K}$ are not presented. Equation (35) can be reduced to an eigenvalue problem with respect to C_{mkq} alone, from which we determine the eigenfrequencies and associated eigenmodes.

Mechanical Model

The mechanical models shown in Figs. 2a and 2b are developed for the first two modes, one of which has a predominant motion in the $\tilde x\tilde z$ plane while the other predominantly oscillates in the $\tilde y$ direction. These two modes are referred to as the $\tilde x$ mode and $\tilde y$ mode, respectively, in this paper.

Explanation is given for the $\tilde x$ mode only, because the method is similar for both the modes. The admissible functions for p_{slo}, u_R,

u_θ, u_φ, and ζ can be expressed in terms of the mode shape functions determined in the preceding section:

$$p_{\text{slo}}(R, \theta, \varphi, t) = -\rho a \ddot{q}(t) \bar{p}_{\text{slo}}(R, \theta, \varphi) \tag{36}$$

$$u_R(R, \theta, \varphi, t) = aq(t)\bar{u}_R(R, \theta, \varphi) \tag{37a}$$

$$u_\theta(R, \theta, \varphi, t) = aq(t)\bar{u}_\theta(R, \theta, \varphi) \tag{37b}$$

$$u_\varphi(R, \theta, \varphi, t) = aq(t)\bar{u}_\varphi(R, \theta, \varphi) \tag{37c}$$

$$\zeta(\theta, \varphi, t) = q(t)\bar{\zeta}(\theta, \varphi) \tag{38}$$

where $q(t)$ represents the modal coordinate. Substituting Eqs. (36–38) into the variational principle [Eq. (26)] and considering the variation with respect to $q(t)$ leads to the following modal equation:

$$\ddot{q} + (\omega_{\tilde{x}})^2 q = \beta_{\tilde{x}} \ddot{f}_{\tilde{x}}(t) + \beta_{\tilde{y}} \ddot{f}_{\tilde{y}}(t) \cong \beta_{\tilde{x}} \ddot{f}_{\tilde{x}}(t) \tag{39}$$

The slosh force and moment are calculated by integrating the appropriate components of the dynamic liquid pressure $p_{\text{slo}} + p_{\text{imp}}$ and are expressed of the form

$$F_{\tilde{x}} = A\ddot{q} + B\ddot{f}_{\tilde{x}}(t) \tag{40}$$

$$M_{\tilde{y}} = C\ddot{q} + D\ddot{f}_{\tilde{x}}(t) \tag{41}$$

The slosh moment is taken about the apex of the conical part of the tank.

For brevity, constants A, B, C, and D are not presented here. The frequency responses of the slosh force and moment to the sinusoidal excitation

$$\ddot{f}_{\tilde{x}}(t) = \sin \omega t \tag{42}$$

can be calculated as

$$F_{\tilde{x}} = \frac{\omega^2(A\beta_{\tilde{x}} + B) - (\omega_{\tilde{x}})^2 B}{\omega^2 - (\omega_{\tilde{x}})^2} \sin \omega t \tag{43}$$

$$M_{\tilde{y}} = \frac{\omega^2(C\beta_{\tilde{x}} + D) - (\omega_{\tilde{x}})^2 D}{\omega^2 - (\omega_{\tilde{x}})^2} \sin \omega t \tag{44}$$

For the mechanical model (Fig. 2a), the frequency responses of the force and moment to the sinusoidal excitation [Eq. (42)] are given by

$$F_{\tilde{x},\text{mech}} = \frac{m_{0\tilde{x}}\left[(\omega_{\tilde{x},\text{mech}})^2 - \omega^2\right] + k_{\tilde{x}}}{\omega^2 - (\omega_{\tilde{x},\text{mech}})^2} \sin \omega t \tag{45}$$

$$M_{\tilde{y},\text{mech}} = \frac{m_{0\tilde{x}} l_{0\tilde{x}}\left[(\omega_{\tilde{x},\text{mech}})^2 - \omega^2\right] + k_{\tilde{x}} l_{1\tilde{x}} + m_{1\tilde{x}} g \cos\gamma}{\omega^2 - (\omega_{\tilde{x},\text{mech}})^2} \sin \omega t \tag{46}$$

where

$$\omega_{\tilde{x},\text{mech}} = (k_{\tilde{x}}/m_{1\tilde{x}})^{\frac{1}{2}} \tag{47}$$

The derivation of Eqs. (45) and (46) is explained in Appendix B. The dynamic similarity condition

$$F_{\tilde{x}} = F_{\tilde{x},\text{mech}}, \qquad M_{\tilde{y}} = M_{\tilde{y},\text{mech}} \tag{48}$$

requires

$$m_{1\tilde{x}} = A\beta_{\tilde{x}} \tag{49}$$

$$k_{\tilde{x}} = m_{1\tilde{x}}(\omega_{\tilde{x}})^2 \tag{50}$$

$$m_{0\tilde{x}} = -A\beta_{\tilde{x}} - B \tag{51}$$

$$l_{0\tilde{x}} = -(C\beta_{\tilde{x}} + D)/m_{0\tilde{x}} \tag{52}$$

$$l_{1\tilde{x}} = \left[(\omega_{\tilde{x}})^2 C\beta_{\tilde{x}} - m_{1\tilde{x}} g \cos\gamma\right]\Big/ k_{\tilde{x}} \tag{53}$$

from which the parameters of the mechanical model (Fig. 2a) can be determined.

Numerical Results

The numerical calculation is performed for the following case: $a = 0.25$ m, $\theta_C = 40$ deg, $\gamma = 43$ deg, $L = 0.765$ m, $H = 0.284$ m, $g = 2$ m/s^2, $\alpha = 0$ (see Fig. 1), and $\rho = 1009$ kg/m^3. The results for this case are illustrated in Fig. 5, showing the nondimensional slosh masses (Fig. 5a), the dimensional slosh masses (Fig. 5b), and the attachment positions of the slosh and fixed masses (Fig. 5c) as functions of the liquid-filling level. These results are shown using solid and dash-dot lines for the $\tilde{x}$ and $\tilde{y}$ modes, respectively.

It can be seen from Fig. 5a that for low liquid-filling levels, $m_{1\tilde{x}}/m_{\text{liquid}}$ is larger than $m_{1\tilde{y}}/m_{\text{liquid}}$. We attribute this to the following reasons: 1) the strong curvature of the conical tank wall around the $\tilde{z}$ axis in the vicinity of the apex of the cone has a constraining effect on the slosh motion in the $\tilde{y}$ direction; and 2) the presence of the conical part and the tilt $\gamma \cong 45$ deg (see Fig. 1) of the tank axis $\tilde{z}$ from the z axis render the liquid surface longer in the x' direction than in the $\tilde{y}$ direction. Consequently, the dynamic liquid pressure applied along the generatrix of the tank wall nearest to the z axis contributes a predominant portion to the resultant slosh force $F_{\tilde{x}}$. Thus, the presence of the conical part has entirely different influences on the $\tilde{x}$ and $\tilde{y}$ modes for low liquid-filling levels, that is, lower than 40%.

As can be seen from Fig. 5b, the actual values of the slosh masses $m_{1\tilde{x}}$ and $m_{1\tilde{y}}$ are small for low liquid-filling levels because the total liquid mass is small. The small values of the slosh masses for high liquid-filling levels are attributed to the decrease in the area of the liquid surface M, which results in the reduction of the kinematic energy of the liquid relative to the tank given by

$$\frac{1}{2}\iiint_V (\nabla\phi)^2 \, dV = \frac{1}{2}\left(-\iint_M \phi \frac{\partial\phi}{\partial N_M} dM + \iint_W \phi \frac{\partial\phi}{\partial N_W} dW\right) \tag{54}$$

where the integral over the tank wall W is zero in Eq. (18). Thus, the slosh masses $m_{1\tilde{x}}$ and $m_{1\tilde{y}}$ are small for both high and low liquid-filling levels and consequently exhibit a maximum value at a certain intermediate value of the liquid-filling level.

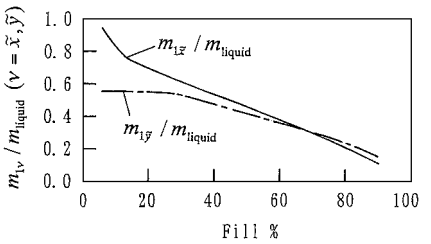

a) Nondimensional slosh mass

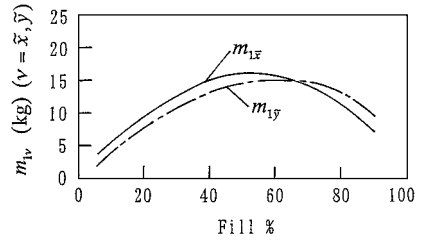

b) Dimensional slosh mass

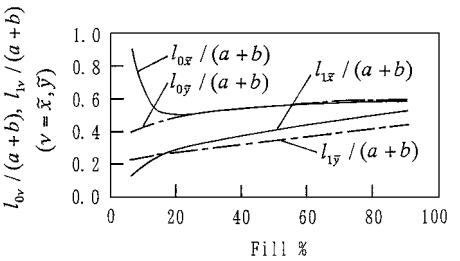

c) Attachment positions of slosh and fixed masses

Fig. 5 Numerical results.

It can be seen from Fig. 5c that $l_{0\tilde{x}}$ takes large values for extremely low liquid-filling levels. The reason for this can be explained as follows: The ratio $m_{1\tilde{x}}/m_{\text{liquid}}$ is close to 1, as shown in Fig. 5a. Hence, the ratio of the fixed mass to the total liquid mass $m_{0\tilde{x}}/m_{\text{liquid}} = 1 - (m_{1\tilde{x}}/m_{\text{liquid}})$ is small. For low liquid-filling levels, m_{liquid} is small, and therefore the fixed mass $m_{0\tilde{x}}$ is very small. This results in a small value of the denominator in Eq. (52) and hence a large value of $l_{0\tilde{x}}$.

Another point of interest is that, only for very low liquid-filling levels, $l_{1\tilde{x}}$ is smaller than $l_{1\tilde{y}}$. This is due to the contribution of the second term $m_{1\tilde{x}} g \cos\gamma$ of the numerator in Eq. (53) to $l_{1\tilde{x}}$. In fact, if we neglect this term, we are led to the conclusion that $l_{1\tilde{x}}$ is larger than $l_{1\tilde{y}}$ for all the liquid-filling levels. The term $m_{1\tilde{x}} g \cos\gamma$ for the $\tilde{x}$ mode [Eq. (53)] is replaced by $m_{1\tilde{y}}\ g \cos\gamma$ for the $\tilde{y}$ mode. Since $m_{1\tilde{x}} > m_{1\tilde{y}}$ for low liquid-filling levels (Fig. 5a), $l_{1\tilde{x}}$ is smaller than $l_{1\tilde{y}}$.

Conclusions

An improved method of solving the sloshing problem with an nonaxisymmetrical shape of the static liquid domain was presented. As an example, sloshing in a teardrop tank was considered under the condition that the propulsive acceleration is predominant to the centrifugal and Coriolis accelerations. It was shown that the application of spherical coordinates according to the position of the contact line of the liquid surface with the tank wall makes it possible to determine the characteristic functions analytically. The use of the Euler angles to determine the relation between the spherical coordinates and the tank-fixed Cartesian coordinates facilitates the mathematical expression of the liquid surface for high liquid-filling levels. When the spherical coordinates are used, the characteristic functions can be obtained by solving a Sturm–Liouville-type boundary value problem for each subdivided section, although the liquid domain shape is geometrically complicated because of the large tilt of the tank axis from the geometrical centerline of the tank system. The solution can be expressed in terms of the Gaussian hypergeometric series with rapid convergence ability. Using the Galerkin method with admissible functions constituted by the characteristic functions, the governing differential equations were transformed into modal equations that were used to develop a mechanical model. Numerical results were presented and discussed for mechanical models developed in two orthogonal directions normal to the tank axis.

Acknowledgments

This work was motivated by the development of the lunar exploration satellite LUNAR-A. The author is grateful to M. Kono and other members associated with the LUNAR-A project at the Institute of Space and Astronautical Science in Sagamihara, Kanagawa Prefecture, Japan.

Appendix A: Derivation of the Characteristic Functions [Eqs. (32) and (33)]

In spherical coordinates, the Laplace equation for p_{slo} can be expressed as

$$\frac{\partial^2 p_{\text{slo}}}{\partial R^2} + \frac{2}{R}\frac{\partial p_{\text{slo}}}{\partial R} + \frac{1}{R^2}\frac{\partial^2 p_{\text{slo}}}{\partial \theta^2} + \frac{\cot\theta}{R^2}\frac{\partial p_{\text{slo}}}{\partial \theta} + \frac{1}{R^2 \sin^2\theta}\frac{\partial^2 p_{\text{slo}}}{\partial \varphi^2} = 0 \tag{A1}$$

The solution of Eq. (A1) must be expressed as a linear combination of characteristic functions that are orthogonal within the range $0 \le \theta \le \bar{\theta}$. Because $\bar{\theta} < \pi/2$ (see Fig. 4), such an orthogonality condition cannot be satisfied by the commonly used associated Legendre polynomials. This impossibility is the reason why the characteristic functions must be derived anew here.

We assume a solution in terms of separated variables, that is,

$$p_{\text{slo}}(R, \theta, \varphi, t) = X(R)\Theta(\theta)\Phi_{mq}(\varphi)e^{i\omega t} \tag{A2}$$

where $\Phi_{mq}(\varphi)$ is given by Eq. (34). Substituting Eq. (A2) into Eq. (A1) gives

$$\frac{d^2X}{dR^2} + \frac{2}{R}\frac{dX}{dR} - \frac{\lambda}{R^2}X = 0 \tag{A3}$$

$$\frac{d^2\Theta}{d\theta^2} + \cot\theta\frac{d\Theta}{d\theta} + \left(\lambda - \frac{m^2}{\sin^2\theta}\right)\Theta = 0 \tag{A4}$$

Substituting $X = R^\alpha$ into Eq. (A3), we obtain

$$\alpha(\alpha + 1) = \lambda \tag{A5}$$

On the other hand, Eq. (A4) is solved for the boundary condition

$$\frac{d\Theta}{d\theta} = 0 \quad \text{at} \quad \theta = \bar{\theta} \tag{A6}$$

to determine the characteristic function Θ_{mk} and the associated characteristic value λ_{mk}. The boundary condition [Eq. (A6)] is a consequence of Eq. (18) because at $\theta = \bar{\theta}$, the θ direction coincides with the normal of the tank wall (see Fig. 4). Thus, the local satisfaction [Eq. (A6)] of the boundary condition [Eq. (18)] determines the admissible function used for the Galerkin method.

The new variables

$$\xi = \cos\theta, \qquad u(\xi) = (1 - \xi^2)^{-m/2}\Theta(\theta) \tag{A7}$$

transform Eq. (A4) into

$$\frac{d^2u}{d\xi^2} - \frac{2(m+1)\xi}{1-\xi^2}\frac{du}{d\xi} + \frac{\lambda - m(m+1)}{1-\xi^2}u = 0 \tag{A8}$$

which can be solved using the power-series expansion method. Substituting

$$u(\xi) = (\xi - 1)^\rho \sum_{i=0}^{\infty} a_i(\xi - 1)^i \tag{A9}$$

into Eq. (A8), we obtain an equation for ρ, namely

$$\rho(\rho + m) = 0 \tag{A10}$$

and a recurrence relation for the coefficients a_i:

$$a_{i+1} = \frac{\lambda - i(i+1) - m(m+1+2i)}{2(i+1)(i+1+m)}a_i \tag{A11}$$

Equation (A10) admits $\rho = 0$ for the bounded solution [Eq. (A9)] at $\xi = 1 (\theta = 0)$. The characteristic values $\lambda = \lambda_{mk} (k = 1, 2, \ldots)$ can be determined from Eq. (A6). The relation [Eq. (A5)] transforms Eq. (A11) into

$$a_{i+1} = \frac{-(m - \alpha + i)(\alpha + m + 1 + i)}{2(i+1)(m+1+i)}a_i \tag{A12}$$

which can be used to express the required characteristic function in terms of the Gaussian hypergeometric series as Eq. (33). The characteristic exponent in the R-dependent function in Eq. (32) can be determined from Eq. (A5) as

$$\alpha_{mk1} = \tfrac{1}{2}\left(-1 - \sqrt{1 + 4\lambda_{mk}}\right), \qquad \alpha_{mk2} = \tfrac{1}{2}\left(-1 + \sqrt{1 + 4\lambda_{mk}}\right) \tag{A13}$$

The normalization parameters $L_l (l = 1, 2)$ in Eq. (32) are introduced to improve the convergence of the series [Eq. (30)]. Namely, as k increases, $\lambda_{mk} \to \infty$, that is, $\alpha_{mk1} \to -\infty$ and $\alpha_{mk2} \to \infty$. Consequently, L_1 and L_2 are, respectively, the minimum and maximum values of R considered.

Appendix B: Derivation of Eqs. (45) and (46)

Equations (1) and (2) are combined to obtain the relation between the coordinate systems $Cxyz$ and $\tilde{O}\tilde{x}\tilde{y}\tilde{z}$:

$$\begin{Bmatrix} x \\ y \\ z \end{Bmatrix} = \begin{bmatrix} -\cos\alpha\cos\gamma & -\sin\alpha & -\cos\alpha\sin\gamma \\ -\sin\alpha\cos\gamma & \cos\alpha & -\sin\alpha\sin\gamma \\ \sin\gamma & 0 & -\cos\gamma \end{bmatrix} \begin{Bmatrix} \tilde{x} \\ \tilde{y} \\ \tilde{z} \end{Bmatrix} + \begin{Bmatrix} L\cos\alpha \\ L\sin\alpha \\ H \end{Bmatrix} \tag{B1}$$

based on which the following coordinate transformation matrix $\boldsymbol{C}$ can be defined.

$$\boldsymbol{C} \equiv \begin{bmatrix} \cos(\tilde{x}, x) & \cos(\tilde{x}, y) & \cos(\tilde{x}, z) \\ \cos(\tilde{y}, x) & \cos(\tilde{y}, y) & \cos(\tilde{y}, z) \\ \cos(\tilde{z}, x) & \cos(\tilde{z}, y) & \cos(\tilde{z}, z) \end{bmatrix} = \begin{bmatrix} -\cos\alpha\cos\gamma & -\sin\alpha\cos\gamma & \sin\gamma \\ -\sin\alpha & \cos\alpha & 0 \\ -\cos\alpha\sin\gamma & -\sin\alpha\sin\gamma & -\cos\gamma \end{bmatrix} \tag{B2}$$

where (a, b) denotes the angle between the a and b directions.

The disturbed position vector of the slosh mass observed in the $(\tilde{x}, \tilde{y}, \tilde{z})$ coordinates is

$$\tilde{\boldsymbol{r}} = \{\tilde{x}, \tilde{y}, \tilde{z}\}^T = \{u, 0, l_{1\tilde{x}}\}^T \tag{B3}$$

where u represents the dynamical displacement of the slosh mass in the $\tilde{x}$ direction. The gravitational force acting on the slosh mass can be expressed in the (x, y, z) coordinates as

$$\boldsymbol{F} = \{0, 0, m_{1\tilde{x}}g\}^T \tag{B4}$$

The equation of motion of the slosh mass in the $\tilde{x}$ direction is

$$m_{1\tilde{x}}\ddot{u} + k_{\tilde{x}}u = -m_{1\tilde{x}}\ddot{f}_{\tilde{x}}(t) \tag{B5}$$

that is,

$$\ddot{u} + (\omega_{\tilde{x},\text{mech}})^2 u = -\ddot{f}_{\tilde{x}}(t) \tag{B6}$$

where $\omega_{\tilde{x},\text{mech}}$ is defined by Eq. (47). From Eq. (B6), the response of u to the sinusoidal excitation [Eq. (42)] is

$$u = 1\Big/\left[\omega^2 - (\omega_{\tilde{x},\text{mech}})^2\right]\sin\omega t \tag{B7}$$

The dynamical parts of the $\tilde{x}$ component of the force $\tilde{\boldsymbol{F}} = \boldsymbol{CF}$ and the $\tilde{y}$ component of the moment $\tilde{\boldsymbol{r}} \times \tilde{\boldsymbol{F}} = \tilde{\boldsymbol{r}} \times \boldsymbol{CF}$ contribute to the resultant force and moment, respectively, together with the elastic force of the spring and the inertia force due to the fixed mass. Hence, we have

$$F_{\tilde{x},\text{mech}} = k_{\tilde{x}}u - m_{0\tilde{x}}\ddot{f}_{\tilde{x}}(t) \tag{B8}$$

$$M_{\tilde{y},\text{mech}} = k_{\tilde{x}}l_{1\tilde{x}}u - m_{0\tilde{x}}l_{0\tilde{x}}\ddot{f}_{\tilde{x}}(t) + (m_{1\tilde{x}}g\cos\gamma)u \tag{B9}$$

Substituting Eq. (B7) into Eqs. (B8) and (B9) leads to Eqs. (45) and (46).

References

[1] Abramson, H. N. (ed.), *The Dynamic Behavior of Liquids in Moving Containers*, NASA SP-106, 1966.

[2] Utsumi, M., "Low-Gravity Propellant Slosh Analysis Using Spherical Coordinates," *Journal of Fluids and Structures*, Vol. 12, No. 1, 1998, pp. 57–83.

[3] Utsumi, M., "Position of Propellant in Teardrop Tank Systems," *Journal of Spacecraft and Rockets*, Vol. 34, No. 6, 1997, pp. 799–804.

I. E. Vas
Associate Editor